High-order-harmonic generation of vibrating H_2^+ and D_2^+

Dmitry A. Telnov,[1,*] John Heslar,[2,†] and Shih-I Chu[2,3,‡]

[1]*Department of Physics, St. Petersburg State University, 7-9 Universitetskaya naberezhnaya, St. Petersburg 199034, Russia*

[2]*Center for Quantum Science and Engineering, Department of Physics, National Taiwan University, Taipei 10617, Taiwan*

[3]*Department of Chemistry, University of Kansas, Lawrence, Kansas 66045, USA*

(Received 3 March 2017; published 26 April 2017)

We study the isotope effect on high-order-harmonic generation (HHG) of vibrating H_2^+ and D_2^+ molecular ions aligned parallel to the polarization of the laser field. The time-dependent Schrödinger equation is solved accurately and efficiently by the time-dependent generalized pseudospectral and Fourier grid methods in three spatial coordinates, one of them being the internuclear separation and the other two describing the electronic motion. The laser pulses have a carrier wavelength of 800 nm and duration of 10 or 16 optical cycles. The peak intensities used in the calculations are 2×10^{14} and 3×10^{14} W/cm^2. The effect of nuclear vibration is visible in both H_2^+ and D_2^+ but more pronounced in the lighter H_2^+ molecule. Striking differences from the fixed nuclei case are a total disappearance of the traditional plateau in the HHG spectrum at the higher intensity and significant redshift of the harmonic peaks in the central part of the spectrum. These phenomena are explained based on the analysis of the dynamics of the nuclear vibrational wave packet.

DOI: 10.1103/PhysRevA.95.043425

I. INTRODUCTION

High-order-harmonic generation (HHG) is a fundamental strong-field process in atoms, molecules, and solids attracting much attention due to its applications in science and technology [1]. Closely related to HHG is generation of attosecond pulses [2,3], opening a road to the attosecond optics [4]. Other applications of HHG include ultrafast spectroscopy and molecular imaging [5,6], a possible tool for probing the electronic and nuclear motion. Usually, the conversion efficiency of HHG of photon energies above the ionization threshold of the target atom or molecule (above-threshold harmonics) is quite low (of the order of 10^{-6}); thus growing attention has been attracted recently to near- and below-threshold harmonics as a potential high-average-power light source in the vacuum ultraviolet band [7–10] (see also a recent review [11] and references therein).

The basic mechanisms and theoretical foundations of HHG are well understood following the work of Corkum [12] and Lewenstein *et al.* [13]. The emission of the harmonic radiation is caused by the electronic motion, which is generally much faster than the nuclear motion in molecules; therefore neglecting the nuclear degrees of freedom seems to be a reasonable approach. The fixed-nuclei approximation has been used in many theoretical studies of molecular HHG (see, for example, [14–17]). Within this approximation, important phenomena such as two-center interference and the dependence of the HHG signal on the orientation of the molecular axis with respect to the polarization of the laser field have been successfully studied [15,18,19]. On the other hand, the time scale of the nuclear vibration can be as short as 10–20 fs and is comparable to the duration of driving laser pulses; thus the nuclear dynamics during the interaction of the molecule with the laser field can influence electronic processes such as HHG and multiphoton ionization. This influence can be significant, as confirmed experimentally [20–26].

Due to the extra degrees of freedom, even the simplest diatomic molecules show a considerably more complicated response to strong fields than that of atoms and pose an additional challenge to the theory. Accurate *ab initio* treatment of all electronic and nuclear degrees of freedom is still beyond the capabilities of modern computational equipment even for one-electron diatomic molecules. Most of the existing theoretical and computational studies on molecular HHG that treat both electronic and nuclear motion are based on simplified models involving the Born-Oppenheimer approximatio [27–30] (for consistent formulation of the time-dependent Born-Oppenheimer approximation, see Refs. [31,32]) or reduced dimensionality [33–35]. The theories of Refs. [29,30] treat the harmonic yield as the sum of contributions corresponding to different internuclear separations weighted by the nuclear wave-packet distribution. It was observed that the harmonic signal is very sensitive to the bond length [29], so an accurate description of the nuclear dynamics including nonadiabatic effects is important. One of the early studies beyond the Born-Oppenheimer approximation [36] reported the HHG spectra of dissociating H_2^+ at a driving laser wavelength of 600 nm and indicated that the dominant contribution to the HHG signal comes from large internuclear distances. A model that incorporates the internal vibrational degrees of freedom in molecules was presented in Refs. [37,38] and was applied to the description of HHG processes in SF_6. A theory of short-time nuclear autocorrelation functions in polyatomic molecules [39,40] was used to explain the isotope and nonadiabatic coupling effects. Another theoretical framework for HHG in complex molecules and clusters [41] is based on the time-dependent density functional theory and includes the effect of nuclear dynamics as well as nonadiabatic couplings between the electronic states. The isotope effects in water and ammonia molecules were studied numerically in Refs. [42,43], respectively. More recently, theoretical investigations [44–51] confirmed that HHG in vibrating molecules may be very different from those in the fixed nuclei approximation and pointed out some interesting

*d.telnov@spbu.ru
†john.heslar@gmail.com
‡sichu@ku.edu

phenomena such as a redshift in the HHG spectra [44,46] and the possible generation of even harmonics [48,49,51].

In this paper, we study the isotope effect on HHG of vibrating H_2^+ and D_2^+ molecular ions aligned parallel to the polarization of the laser field. Our approach treats the electronic motion in full dimensionality and includes nonadiabatically the effect of nuclear vibration. Only the nuclear rotation is neglected, but its effect may not be very important for aligned molecules on the femtosecond time scale. Our calculations reveal qualitative differences of the HHG spectra due to the nuclear motion, such as transformation of the HHG plateau and redshift of the harmonic peaks, compared to the fixed-nuclei case. We analyze these phenomena and compare the effect of nuclear vibration in H_2^+ and D_2^+, emphasizing the role of the vertical ionization potential, which depends on the internuclear distance and varies during the interaction of the molecule with the laser pulse.

This paper is organized as follows. In Sec. II, we briefly discuss our theoretical and computational approach; a detailed description of the method can be found in our previous paper [47]. In Sec. III we present our results regarding the dynamics of the nuclear wave packet and HHG spectra, compare the behaviors of H_2^+ and D_2^+, and provide an in-depth discussion of the key phenomena. Section IV contains concluding remarks.

II. METHOD

A detailed description of our theoretical and computational approach is given elsewhere [47]. Here we briefly outline the key points. We use Jacobi coordinates to describe one-electron diatomic systems H_2^+ and D_2^+. The Jacobi coordinates are the relative radius vector of the nuclei $\boldsymbol{R}$, the radius vector of the electron with respect to the center of mass of the nuclei $\boldsymbol{r}$, and the radius vector of the center of mass of the whole system $\boldsymbol{R}_c$. First, the center-of-mass motion can be separated; thus only the coordinates $\boldsymbol{R}$ and $\boldsymbol{r}$ remain. Second, in the linearly polarized laser field, we consider only the molecules aligned parallel to the polarization vector of the field and neglect the nuclear rotation. Then the direction of the vector $\boldsymbol{R}$ (molecular axis) is fixed in space, and only its length (the internuclear distance R) describes the nuclear vibration. Third, for the laser field polarized along the molecular axis (let us denote it the z axis), the projection m_z of the electron angular momentum on the molecular axis is conserved, and the electronic coordinate describing rotation about the z axis can be eliminated. The remaining problem is three-dimensional (3D; one nuclear and two electronic degrees of freedom). The total Hamiltonian, including the kinetic-energy operator and interaction with the laser field in the dipole approximation (length gauge), can be represented as follows [47]:

$$H(t) = H_0 + V(t), \tag{1}$$

$$H_0 = -\frac{1}{M}\left[\frac{\partial^2}{\partial R^2} + \frac{2}{R}\frac{\partial}{\partial R}\right] + \frac{1}{R} - \frac{2}{\mu R^2}\frac{1}{(\xi^2-\eta^2)}\left[\frac{\partial}{\partial\xi}(\xi^2-1)\frac{\partial}{\partial\xi} + \frac{\partial}{\partial\eta}(1-\eta^2)\frac{\partial}{\partial\eta} - \frac{m_z^2}{\xi^2-1} - \frac{m_z^2}{1-\eta^2}\right] - \frac{4\xi}{R(\xi^2-\eta^2)}, \tag{2}$$

$$V(t) = \frac{1}{2}\left(1+\frac{m}{2M+m}\right)F(t)R\xi\eta. \tag{3}$$

In Eqs. (2) and (3), ξ and η are the prolate spheroidal coordinates of the electron radius vector $\boldsymbol{r}$ (with the foci of the prolate spheroidal coordinate system situated on the nuclei), M and m are the single nucleus and electron mass, respectively, and μ is the reduced electron mass:

$$\mu = \frac{2Mm}{2M+m}. \tag{4}$$

The notation $F(t)$ stands for the electric field strength of the laser field.

The time-dependent Schrödinger equation

$$i\frac{\partial}{\partial t}\Psi(\xi,\eta,R,t) = H(t)\Psi(\xi,\eta,R,t) \tag{5}$$

for the Hamiltonian (1) is solved using the time-dependent generalized pseudospectral method (TDGPS) [52]. The coordinates ξ and η are discretized with the help of the generalized pseudospectral (GPS) method, applying the Gauss-Legendre set of collocation points for η and the Gauss-Radau set for ξ [19,53]. For discretization of the R coordinate, we apply the Fourier grid (FG) method [54]. For the time evolution of the wave function, we employ the following split-operator, second-order, short-time propagation formula:

$$\Psi(t+\Delta t) = \exp\left(-\frac{i}{2}\Delta t\, H_0\right)\exp\left[-i\,\Delta t\, V\left(t+\frac{1}{2}\Delta t\right)\right] \times \exp\left(-\frac{i}{2}\Delta t\, H_0\right)\Psi(t). \tag{6}$$

Here Δt is the time propagation step. The operator $\exp(-\frac{i}{2}\Delta t\, H_0)$ is constructed by the spectral expansion:

$$\exp\left(-\frac{i}{2}\Delta t\, H_0\right) = \sum_n \exp\left(-\frac{i}{2}\Delta t\, E_n\right)|\psi_n\rangle\langle\psi_n|, \tag{7}$$

where ψ_n and E_n are the eigenvectors and eigenvalues, respectively, of the unperturbed Hamiltonian H_0 (2). In practical calculations, the summation in (7) includes all eigenvectors with energies $E_n < E_b$, where the upper limit E_b should be large enough to describe all relevant physical processes. With the control of high-energy contributions to the propagator matrix, we can avoid population of physically irrelevant regions of the energy spectrum and improve the numerical stability of the computations. In the present work, we use $E_b = 10$ a.u. For a carrier wavelength of 800 nm and a peak intensity of 3×10^{14} W/cm^2, this value of E_b is approximately equal to $15U_p$ (U_p is the ponderomotive potential), which is well in excess of the expected cutoff energy of the HHG spectrum. For the given Δt, the propagator matrix $\exp(-\frac{i}{2}\Delta t\, H_0)$ is time independent and constructed only once before the propagation process starts. The matrix $\exp[-i\,\Delta t\, V(t+\frac{1}{2}\Delta t)]$ is time dependent and must be calculated at each time step. However, for the interaction with the laser field in the length gauge, this matrix is diagonal in both the GPS and FG methods, and its calculation is not time-consuming (all potential terms are represented by their values on the coordinate grid and appear as diagonal matrices; no calculation of potential-energy matrix elements is required).

TABLE I. Low-lying vibrational eigenvalues of H_2^+ and D_2^+ (a.u.). Here A indicates the present calculations for aligned molecules with no rotation, and B indicates the fully nonadiabatic rovibrational eigenvalues for the total angular momentum $J = 0$ [55].

	H_2^+		D_2^+	
v	A	B	A	B
0	−0.59723	−0.59714	−0.59883	−0.59879
1	−0.58725	−0.58716	−0.59165	−0.59160
2	−0.57785	−0.57775	−0.58485	−0.58471
3	−0.56899	−0.56891	−0.57816	−0.57811
4	−0.56064	−0.56061	−0.57107	−0.57179
5	−0.55297	−0.55284	−0.56695	−0.56574

The problem is solved in a box with a linear dimension of $r_b = 43$ a.u. for the electronic motion. The box size must be large enough to accommodate electron excursions in the laser field (the excursion amplitude does not exceed 29 a.u. for the chosen field parameters); on the other hand, it should be kept as small as possible to make the calculations more accurate with the same number of grid points. We performed several tests in the two-dimensional fixed-nuclei computational scheme (which requires much less computer memory and time) while varying r_b and found that $r_b = 43$ a.u. is enough for convergence of the HHG spectra up to a harmonic order of 65, which is the cutoff region at $R = 2$ a.u. and an intensity of 3×10^{14} W/cm^2. In our 3D calculations, the internuclear distance R is restricted to the interval [0.75,8.75], which is large enough to contain the nuclear wave packet during the laser pulse. To achieve sufficient accuracy, we use 96 grid points in ξ, 24 grid points in η, and 31 grid points in R (the total linear dimension of the Hamiltonian matrix is 71 424). In the present work, we use 4096 time steps per optical cycle; this is enough to achieve convergence for the wavelength and intensity used in the calculations. In intense laser fields, ionization can be significant. In our present calculations, the ionized parts of the electronic wave packet are collected by an absorbing layer placed near the boundary r_b. Because of the absorber, the normalization of the wave function decreases in time. The ionization probability can be calculated from the normalization of the wave function at the end of the laser pulse.

III. RESULTS AND DISCUSSION

First, we solve the time-independent Schrödinger equation for the Hamiltonian H_0 (2) and obtain the unperturbed energy eigenvalues and eigenfunctions of H_2^+ and D_2^+. The low-lying energy eigenvalues are listed in Table I (the results for H_2^+ were previously reported in Ref. [47]). As one can see, our energies are in good agreement with the corresponding rovibrational eigenvalues for the total angular momentum $J = 0$ from the accurate variational calculations [55] but slightly lower since we do not include the rotational degrees of freedom. Then the eigenvalues and eigenfunctions are used to construct the short-time propagator in Eq. (7).

The laser pulse $F(t)$ used in our calculations has a $\sin^2$ envelope with a carrier wavelength of 800 nm. We report the results for total durations of 10 optical cycles (o.c.) and 16 o.c. [that is, 26.7 and 42.7 fs, respectively] and peak intensities of

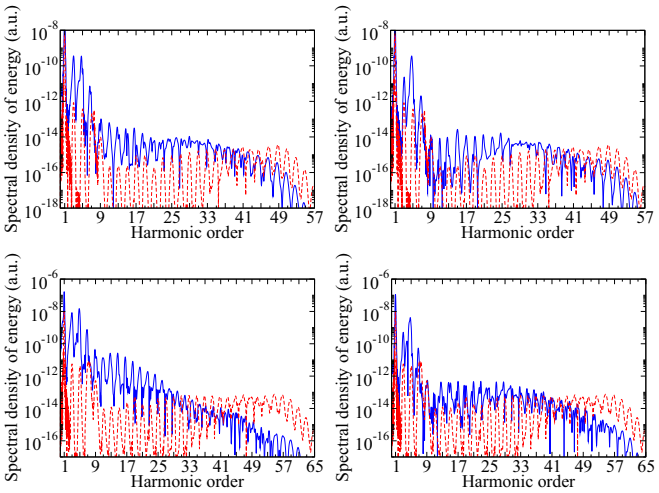

FIG. 1. HHG spectra of H_2^+ (left) and D_2^+ (right) initially in the ground state ($v = 0$) for a peak intensity of the laser field of 2×10^{14} W/cm^2 (top panels) and 3×10^{14} W/cm^2 (bottom panels). Pulse duration is 10 optical cycles. The red dashed line in all panels shows the spectrum for the nuclei fixed at $R = 2$ a.u.

2×10^{14} and 3×10^{14} W/cm^2. With the total time-dependent electron and nuclear wave function $\Psi(\xi,\eta,R,t)$ we can calculate the spectrum of emitted harmonics and analyze the motion of the nuclear wave packet. The HHG spectra are calculated according to the widely used semiclassical approach, where the basic expressions come from classical electrodynamics but the classical quantities such as the dipole moment and its acceleration are replaced with the corresponding quantum expectation values. The spectral density of the radiation energy is given by the following expression [56]:

$$S(\omega) = \frac{2}{3\pi c^3}|\tilde{\boldsymbol{a}}(\omega)|^2, \tag{8}$$

$$\tilde{\boldsymbol{a}}(\omega) = \int_{-\infty}^{\infty} dt\, \boldsymbol{a}(t)\exp(i\omega t), \tag{9}$$

where c is the speed of light. The time-dependent dipole acceleration $\boldsymbol{a}(t)$ is calculated with the help of the Ehrenfest theorem. Using the Jacobi coordinates, one obtains [47]

$$\boldsymbol{a}(t) = -\frac{M+m}{Mm}\left\langle\Psi\left|\nabla_{\boldsymbol{r}}\left[\frac{1}{\left|\boldsymbol{r}-\frac{1}{2}\boldsymbol{R}\right|}+\frac{1}{\left|\boldsymbol{r}+\frac{1}{2}\boldsymbol{R}\right|}\right]\right|\Psi\right\rangle + \frac{M+2m}{Mm}\boldsymbol{F}(t). \tag{10}$$

In Figs. 1 (10-o.c. pulse) and 2 (16-o.c. pulse), we show the HHG spectra $S(\omega)$ for H_2^+ and D_2^+ initially in the ground state $v = 0$. Also shown are the spectra obtained in the fixed-nuclei approximation at the internuclear distance $R = 2$ a.u., which is close to the equilibrium internuclear separation for both H_2^+ and D_2^+. The HHG spectra for the pulse durations 10 and 16 o.c. generally resemble each other for the same target and peak intensity. As expected, the absolute value of the signal is larger, and the harmonic peaks are more distinct for the longer laser pulse. According to the well-known semiclassical recollision model [12], the cutoff of the HHG spectrum is expected at photon energy $I_p + 3.17U_p$,

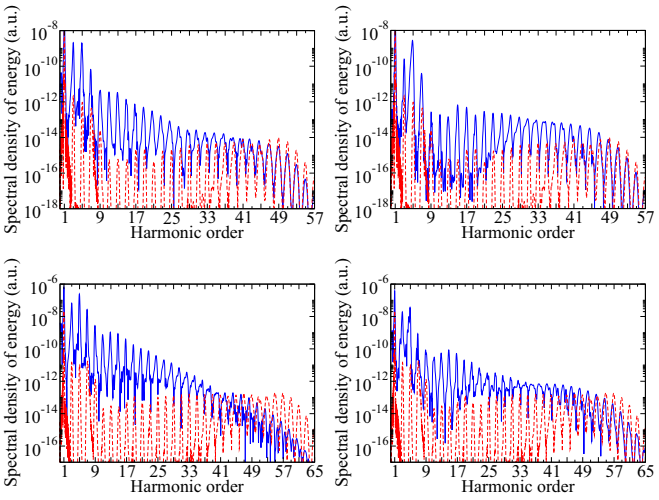

FIG. 2. HHG spectra of H_2^+ (left) and D_2^+ (right) initially in the ground state ($v = 0$) for a peak intensity of the laser field of 2×10^{14} W/cm^2 (top panels) and 3×10^{14} W/cm^2 (bottom panels). Pulse duration is 16 optical cycles. The red dashed line in all panels shows the spectrum for the nuclei fixed at $R = 2$ a.u.

where I_p is the ionization potential of the target. For the vertical ionization potential at $R = 2$ a.u. and peak intensities of 2×10^{14} and 3×10^{14} W/cm^2, the cutoff energy corresponds to harmonic orders 44 and 56, respectively. As one can see, the HHG spectra for the fixed nuclei show sharp cutoffs, in fair agreement with the semiclassical prediction. However, the cutoffs are rather smooth in the case of vibrating nuclei. The most striking difference can be seen in H_2^+ at the higher peak intensity of 3×10^{14} W/cm^2: the traditional plateau in the HHG spectrum totally disappears, and the spectrum manifests a monotonously decreasing pattern. In D_2^+, this phenomenon is less pronounced, although the plateau becomes narrower compared with the fixed-nuclei case for the same laser pulse parameters. Another observation from Figs. 1 and 2 is that the HHG signal from the vibrating molecules is considerably stronger everywhere in the spectrum except for the cutoff region where the situation is reversed. The difference is larger for higher peak intensities and longer pulse durations. In the low-energy and central parts of the spectrum, it is increased from 1–2 orders of magnitude for the 2×10^{14} W/cm^2, 10-o.c. pulse to 3–4 orders of magnitude for the 3×10^{14} W/cm^2, 16-o.c. pulse.

Certainly, the significant difference between the HHG spectra of vibrating molecules and that calculated in the fixed-nuclei approximation is related to the nuclear motion and its influence on the electronic degrees of freedom. That is why it is instructive to study the dynamics of the nuclei in H_2^+ and D_2^+ subject to the laser field. The probability density of the nuclear wave packet $\rho_n(R,t)$ is obtained from the total wave function upon integration over the electronic coordinates:

$$\rho_n(R,t) = \int d^3r |\Psi(\boldsymbol{r},R,t)|^2. \tag{11}$$

The time evolution of the nuclear wave packet is shown in Figs. 3 and 4 for pulse durations of 10 and 16 o.c., respectively. As one can see, when the laser field is switched on, the nuclear

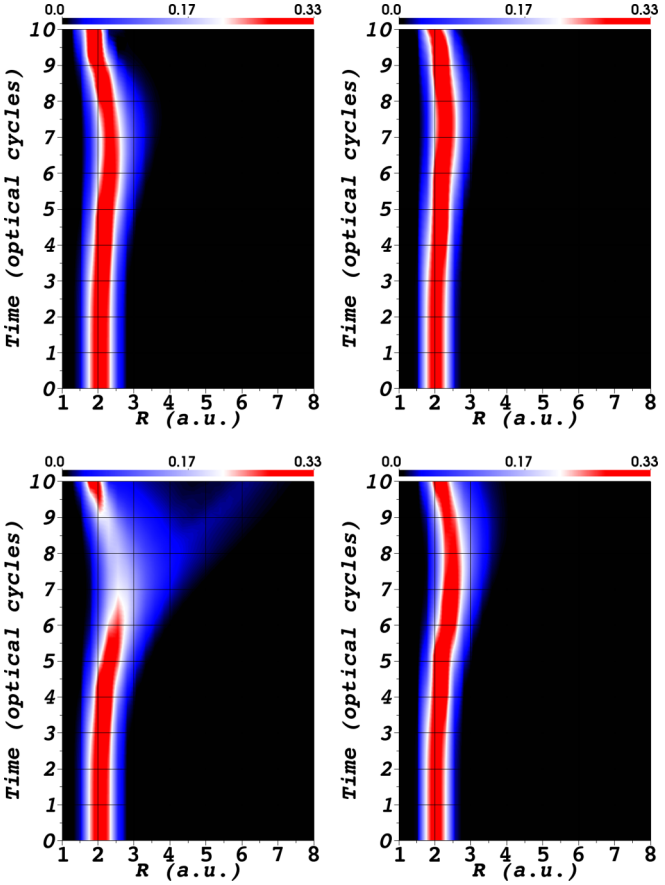

FIG. 3. Time-dependent nuclear density distribution of H_2^+ (left) and D_2^+ (right) initially in the ground state ($v = 0$) for a peak intensity of the laser field of 2×10^{14} W/cm^2 (top panels) and 3×10^{14} W/cm^2 (bottom panels). Pulse duration is 10 optical cycles.

wave packet remains strongly localized around the equilibrium distance $R = 2$ a.u. until the field almost reaches its peak intensity. For the 10-o.c. pulse, noticeable changes begin at about 4 o.c., and for the 16-o.c. pulse they happen at about 7 o.c.; thus the nuclear vibration takes places mainly in the second half of the laser pulse. For the 10-o.c. pulse, a half cycle of vibration is complete by the end of the pulse: the nuclear wave packet goes back to the equilibrium distance for D_2^+ and even smaller distances for H_2^+. For the 16-o.c. pulse, one can also see the second half cycle of the vibration motion, when the wave packet reaches the smallest internuclear separation for both D_2^+ and H_2^+; then it goes again to larger distances for H_2^+. The nuclear vibration is faster for H_2^+; the vibration period T_n of the nuclear wave packet can be estimated as 15 fs, according to the equation $T_n = 2\pi/\omega_n$, where the frequency ω_n is calculated as the difference between the energies of the levels with $v = 1$ and $v = 0$ (see Table I). For D_2^+, $T_n \approx 21$ fs. The ratio of the vibration periods of D_2^+ and H_2^+ calculated using the eigenvalue data from Table I (approximately equal to $\sqrt{2}$) is in full agreement with that based on the nuclear mass ratio. The vibration amplitude and spreading of the nuclear wave packet are larger for H_2^+ for the same peak intensity and pulse duration. At the higher peak intensity of 3×10^{14} W/cm^2, one can clearly see a substantial portion of the nuclear wave packet corresponding to dissociation for both pulse durations

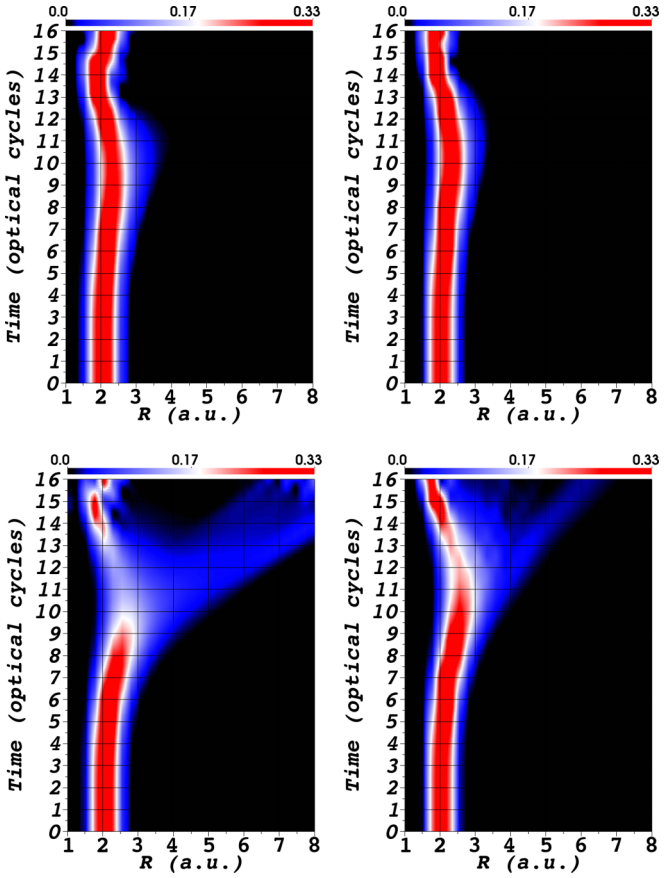

FIG. 4. Time-dependent nuclear density distribution of H_2^+ (left) and D_2^+ (right) initially in the ground state ($v = 0$) for a peak intensity of the laser field of 2×10^{14} W/cm^2 (top panels) and 3×10^{14} W/cm^2 (bottom panels). Pulse duration is 16 optical cycles.

(Figs. 3 and 4). For D_2^+, the dissociation is visible only for the 16-o.c. pulse (Fig. 4), and it is weaker than for H_2^+.

The vertical ionization potential is an important parameter that affects HHG in vibrating molecules, as was discussed previously [34]. As Figs. 3 and 4 show, in the course of laser-induced nuclear vibration the molecule spends a substantial amount of time in stretched configurations, where the internuclear distance is larger than the equilibrium value of $R = 2$ a.u. In the adiabatic Born-Oppenheimer picture, the vertical ionization potential of the ground electronic state $1\sigma_g$ is monotonously decreasing with increasing internuclear separation, varying from $I_p = 2$ a.u. at $R = 0$ to $I_p = 0.5$ a.u. at $R \to \infty$. At the equilibrium distance $R = 2$ a.u., it is equal to 1.103 a.u. (there is no difference between H_2^+ and D_2^+ in the fixed-nuclei approximation). In the tunneling ionization regime, which is established in intense near-infrared and midinfrared laser fields, a smaller ionization potential means a larger ionization probability. Because of the high nonlinearity of the process, even small variations of the ionization potential can result in dramatic changes in the ionization probability. In Table II, we report the ionization probabilities of vibrating H_2^+ and D_2^+ after 16-o.c. laser pulses with peak intensities of 2×10^{14} and 3×10^{14} W/cm^2 and compare them with the corresponding ionization probabilities in the fixed-nuclei approximation at $R = 2$ a.u. As can be

TABLE II. Ionization probabilities of H_2^+ and D_2^+ after a 16-optical-cycle laser pulse.

Peak intensity	Fixed nuclei	Vibrating molecule	
(W/cm^2)	$R = 2$ a.u.	H_2^+	D_2^+
2×10^{14}	3.04×10^{-6}	1.13×10^{-3}	1.64×10^{-4}
3×10^{14}	8.17×10^{-5}	5.91×10^{-2}	9.16×10^{-3}

seen, the ionization probability of H_2^+ is larger than that of D_2^+, and both of them are 2 to 3 orders of magnitude larger than the ionization probability for the nuclei fixed at $R = 2$ a.u. According to the three-step model of HHG [12], a larger probability of ionization at the first step means enhanced emission of harmonic radiation at the final step of the process. Based on this simple picture, one can generally expect a higher HHG signal from vibrating molecules compared with that for the nuclei fixed at the equilibrium distance. However, as one can see from Figs. 3 and 4, the nuclear vibration becomes important in the second half of the laser pulse when the peak intensity has already been passed and the laser field becomes weaker with time. Hence there must be an interplay between the decreasing ionization potential and decreasing instantaneous intensity of the field. Besides that, the smaller ionization potential means a smaller cutoff energy, resulting in the suppressed high-energy part of the HHG spectrum. All these factors affect HHG in vibrating molecules.

A deeper insight into the mechanisms involved can be obtained from the time-frequency analysis of the dipole acceleration. In the present study, we use the synchrosqueezing transform (SST) [57], which can reveal more fine structures in the data than the traditional wavelet transform. Previously, SST was successfully applied for analysis of the dynamical origin of below- and near-threshold harmonics in Cs [58] and H_2^+ [59]. Below we shall use the case of H_2^+ in the field with peak intensity of 3×10^{14} W/cm^2 and pulse duration of 10 o.c. as an example which manifests the general properties of HHG in vibrating molecules. The SST of the dipole acceleration in this case is presented in Fig. 5. As one can see, both below- and above-threshold harmonics (the ionization threshold at $R = 2$ a.u. is marked with the yellow horizontal line in Fig. 5) are mostly emitted in the second half of the laser pulse, within a time interval of 6 to 8 o.c. An exception is made by harmonics in the cutoff region (harmonic orders 55 to 63). These harmonics are emitted in the center of the pulse, where the instantaneous intensity is close to its peak value. The SST analysis of the dipole acceleration at different peak intensities and pulse durations for both H_2^+ and D_2^+ produces patterns similar to that seen in Fig. 5. The time-frequency SST analysis thus confirms that the majority of the harmonics (except for the cutoff region) are emitted by vibrating molecules in stretched configurations when the vertical ionization potential is lower than that at the equilibrium internuclear separation. Lower ionization potential favors ionization, which is the first step of the HHG process according to the three-step model [12]; hence the harmonic radiation is enhanced compared with the case of the nuclei fixed at $R = 2$ a.u. Harmonics in the cutoff region for the given laser pulse parameters can be efficiently produced when the instantaneous intensity is close

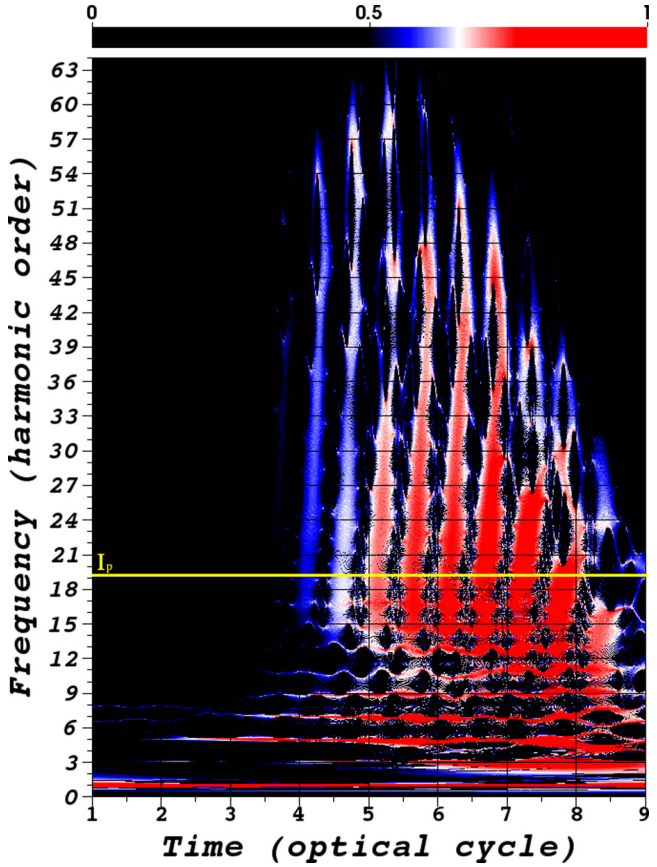

FIG. 5. Time-frequency dipole acceleration SST spectrum of H_2^+ initially in the vibrational states $v = 0$ for a peak intensity of the laser field of 3×10^{14} W/cm^2 and a pulse duration of 10 optical cycles. The horizontal yellow line shows vertical ionization potential at $R = 2$ a.u.

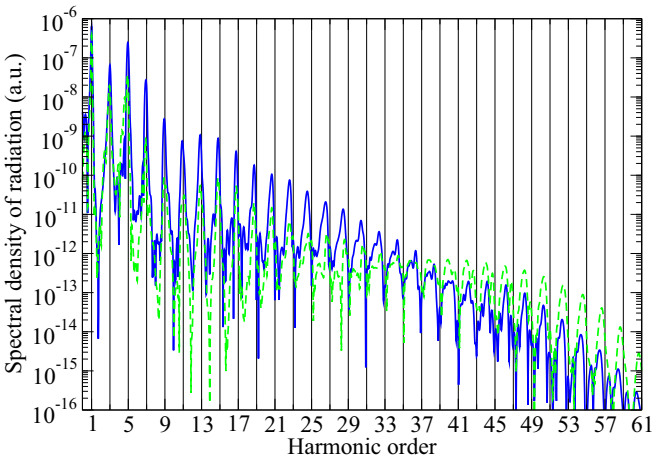

FIG. 6. HHG spectra of H_2^+ (solid blue line) and D_2^+ (dashed green line) initially in the ground state ($v = 0$) for a peak intensity of the laser field of 3×10^{14} W/cm^2 a and pulse duration of 16 optical cycles. Black vertical lines indicate odd harmonic orders.

to its peak value and the vertical ionization potential is still close to the equilibrium value (the cutoff energy is equal to $1.103 + 3.17U_p$, where 1.103 is the vertical ionization potential at $R = 2$ a.u.). For stretched molecules with low vertical ionization potentials, such harmonics lie beyond the cutoff for the particular stretched configuration and are strongly suppressed. Consequently, the condition for efficient generation of the cutoff harmonics in vibrating molecules is satisfied for a shorter period of time than in molecules with the nuclei fixed at the equilibrium internuclear distance. That is why the HHG signal in the cutoff region is stronger in the fixed-nuclei approximation; for vibrating molecules, it is stronger in D_2^+ than in H_2^+ since the nuclei move slower in D_2^+. It was discussed in the literature [22,33] that the HHG signal is generally stronger in heavier isotopes because of slower nuclear motion. The latter results in a more efficient recombination phase since the recombination amplitude is proportional to the overlap between the initial and final nuclear parts of the molecular wave function that evolves from the moment of ionization until the point of recollision [22]. The effect can be quantified through the nuclear autocorrelation function [33]. It was experimentally confirmed for the isotope pair H_2/D_2 [23–26] and was shown to increase towards higher harmonic orders (that is, longer electron travel times between the ionization and recombination), where the measured harmonic intensity in D_2 can be 2 to 3 times larger than the corresponding intensity in H_2. Both the nuclear autocorrelation effect and enhanced ionization are reflected in our calculated HHG spectra, as seen in Figs. 1, 2, and 6. For the laser pulse parameters used in the calculations, the nuclear autocorrelation mechanism can be dominant in the cutoff region where the HHG signal in D_2^+ exceeds that in H_2^+. In the other parts of the spectrum, enhanced ionization due to lower vertical ionization potential in the stretched molecule is more important; thus the HHG signal in H_2^+ is stronger than that in D_2^+ due to the larger vibration amplitude in H_2^+. For relatively long (10 or 16 o.c.) laser pulses it is difficult to cleanly separate the nuclear autocorrelation and enhanced-ionization effects; for this purpose, the pump-probe scheme with short pulses [44] would be preferable.

Another phenomenon observed in the HHG spectra of vibrating molecules is a redshift of the harmonic peaks. In Fig. 6, we show the HHG spectra of H_2^+ and D_2^+ for a peak intensity of 3×10^{14} W/cm^2 and a pulse duration of 16 o.c. Black vertical lines indicate odd harmonic orders where one expects to see the peaks for the systems with inversion symmetry. One can see in Fig. 6 that positions of low-energy harmonic peaks (approximately up to order 15) correspond to odd integer numbers with high accuracy. However, higher harmonics exhibit a noticeable systematic redshift, which becomes very significant for harmonic orders 33 to 47 and can reach the photon energy, so some harmonics in this range have positions close to even harmonic orders. The redshift decreases in the cutoff region (harmonic orders 49 to 61). In the central part of the spectrum (harmonic orders 33 to 47), the redshifts in H_2^+ and D_2^+ are comparable, but for lower and higher harmonics H_2^+ exhibits larger shifts. At a laser peak intensity of 2×10^{14} W/cm^2 (not shown in Fig. 6) the redshift is also present but smaller than that at an intensity of 3×10^{14} W/cm^2. It is worth noting that in the fixed-nuclei approximation there is no redshift, and all harmonic peaks correspond to odd integer harmonic orders.

Previously, the redshift in the molecular HHG spectra was detected in simulations of the pump-probe spectroscopy

scheme [44] and manifested a dependence on the delay time between the pump and probe pulses; it was noted that the shift correlates to the sole contribution of one electron return within one half laser cycle. The probe pulse in Ref. [44], however, was very short (5.3 fs, with a central wavelength of 800 nm); thus discrete harmonics are hardly seen in the spectra. For longer pulses, an appealing explanation for the redshift is a frequency modulation of intercycle HHG dynamics on the falling edge of the laser pulse [46] (see also discussion in Refs. [50,51]). However, this mechanism is related solely to the laser pulse shape and would lead to the redshift of all the harmonics generated predominantly in the second half of the laser pulse, including the low-energy harmonics, and our calculations do not show any significant changes in the positions of the low-energy harmonic peaks. Here we suggest another mechanism behind the redshift in the HHG spectra of vibrating molecules that could contribute to the total redshift along with the frequency modulation effect and could explain different shifts of the harmonics in different parts of the spectrum. According to the three-step model of harmonic generation [12], there is a time delay between the first (ionization) and third (recombination) steps of the process; this time is required for the electron to return to the parental ion following either a short or long trajectory. As revealed by our analysis above, the harmonics are predominantly generated in the part of the laser pulse where the nuclei are still moving apart and the vertical ionization potential is decreasing. That is why the energy released by the electron at the recombination time is smaller than that absorbed from the field at the ionization time. In other words, the energy of the emitted harmonic photon is less than the total energy of the corresponding odd integer number of the carrier photons, leading to the redshift of the peaks in the HHG spectrum. Of course, one should realize that the discrete harmonic spectrum is shaped not by a single recombination event but by interference of contributions from several consecutive optical cycles of the driving laser pulse. The concept of carrier photons with a specific energy is applicable only if the laser pulse contains at least a few optical cycles. When the ionization potential decreases between the ionization and recombination events during several consecutive optical cycles, the radiation energy released at recombination in each optical cycle is less than it would be in the case of a constant ionization potential. Then the interference of the contributions from all these optical cycles forces the energy absorbed from the driving field to be equal to an integer multiple of the carrier photon energy, and the harmonic spectrum is shaped with redshifted discrete harmonics. Since both ionization and recombination steps take place within the same optical cycle, the redshift of the harmonics can be estimated from the variation of the vertical ionization potential during one optical cycle. For the 3×10^{14} W/cm^2, 16-o.c. laser pulse, this variation is about 0.032 a.u., as calculated from the time-dependent expectation value of the internuclear distance during the tenth optical cycle. Hence the variation of the vertical ionization potential has the same order of magnitude as the photon energy (0.057 a.u.) and can contribute considerably to the redshift of the harmonics along with the frequency modulation effect on the falling edge of the laser pulse.

For above-threshold harmonics, where the three-step model is applicable, the actual variation of the vertical ionization potential between the ionization and recombination steps of the HHG process differs for different harmonic orders. As one can see from the time-frequency distribution (Fig. 5), the largest time delays (or the longest trajectories) correspond to the harmonics in the middle of the HHG spectrum, while both high-energy and near-threshold harmonics have smaller emission times within the same optical cycle. Moreover, the cutoff harmonics are generated predominantly at the time when the instantaneous intensity is close to its peak value (that is, in the center of the laser pulse). At this time, the nuclear motion is still quite slow, so the variation of the vertical ionization potential during one optical cycle is insignificant; the frequency modulation effect is also minimal in the center of the pulse. That is why both cutoff and near-threshold harmonics have smaller redshifts than those in the middle of the spectrum. Finally, below-threshold harmonics are not described by the three-step model. Although these harmonics are also predominantly generated in the stretched molecule configuration, when the nuclei are moving apart, there is no noticeable time delay between absorption of the carrier photons and emission of the harmonic photon; thus the variation of the vertical ionization potential does not affect the energy of the emitted photon, and the shift of below-threshold harmonic peaks is much smaller than that of the above-threshold harmonics.

At the end of this section, we would like to comment on generation of even harmonics in vibrating H_2^+ and D_2^+, as recently discussed in the literature [48,49,51] and attributed to dynamical electron localization [48,49] or spatially asymmetric emission along the laser polarization direction [51]. This phenomenon is different from the redshift; the latter, if large enough, can also move the harmonic peak close to the even-order position. Our present calculations do not produce any noticeable even harmonics. In the previous studies of H_2^+ within the fixed-nuclei approximation [60,61], we did see even harmonics at large internuclear separations (5 to 9 a.u.). Generation of even harmonics in this case is well explained by dynamical rupture of symmetry and localization of the electron near one of the nuclei for a substantially long period of time; this mechanism was confirmed by calculations of the time-dependent electron probability density [61]. At large internuclear separations, such a dynamical electron localization is favored by strong coupling between the opposite-parity $1\sigma_g$ and $1\sigma_u$ states (charge resonance effect [62]). In our present calculations, however, the nuclear wave packet does not spread to very large internuclear distances (except for the dissociation channel, which is quite weak for the laser pulse parameters used); thus generation of even harmonics is still suppressed.

IV. CONCLUSION

In this paper, we have studied the isotope effect on high-order-harmonic generation of vibrating H_2^+ and D_2^+ molecular ions subject to laser pulses with a carrier wavelength of 800 nm. The time-dependent wave function of the diatomic molecule aligned parallel to the polarization direction of the laser field depends on three spatial coordinates, including the

internuclear distance and two electronic coordinates. While we neglect rotation of the molecule, the nuclear vibration is treated on the same footing as the full dimensionality electronic motion. The time-dependent Schrödinger equation is solved accurately and efficiently with the help of the time-dependent generalized pseudospectral and Fourier grid methods.

For the laser field frequency, peak intensities, and pulse durations used in our calculations, the spectral density of emitted radiation energy for both H_2^+ and D_2^+ is larger than that in the fixed-nuclei approximation at the equilibrium internuclear distance, except for the cutoff region. The difference is more pronounced for the lighter H_2^+ molecule and eventually results in total disappearance of the traditional HHG plateau at a peak intensity of 3×10^{14} W/cm^2 and pulse duration of 16 o.c. We have explained such transformations of the HHG spectra by variation of the vertical ionization potential in the course of nuclear vibration. When the nuclei are moving apart, the vertical ionization potential is decreasing, leading to both enhancement of ionization as the first step of the HHG process and lowering of the cutoff energy. Consequently, the harmonic radiation is enhanced in the low-energy and central parts of the HHG spectrum but suppressed at higher energies, compared with the fixed-nuclei case. The dramatic difference between the HHG spectra of vibrating and fixed-nuclei molecules must be taken into account in various HHG applications, such as generation of attosecond pulses, where the structure of the HHG plateau is crucial.

Another feature of the HHG spectra related to variation of the vertical ionization potential is the redshift of the harmonic peaks. The largest shift can be seen in the middle of the spectrum and is comparable to the carrier photon energy. Since harmonics are emitted predominantly during the stretching phase of the nuclear vibration, the vertical ionization potential decreases between the ionization and recombination time moments, so the energy released into the harmonic photon at the recombination time is less than the energy absorbed from the laser field at the ionization time. This mechanism contributes to the total redshift along with the frequency modulation effect on the trailing edge of the laser pulse. The shifts are larger for the faster nuclear motion (H_2^+) and smaller for the slower motion (D_2^+); thus the redshift spectroscopy can be used as a tool for probing the nuclear motion.

Our present results were obtained for H_2^+ and D_2^+, the simplest and lightest diatomic molecular systems. In heavier diatomic molecules, one can generally expect that the effects discussed above would be smaller due to slower nuclear motion. However, the nuclear vibration regime strongly depends on the parameters of the driving laser field. In intense fields, where populations of the excited vibrational energy levels and dissociation channel are substantial, transformation of the HHG spectra because of the nuclear motion can still be significant even for heavier molecules.

ACKNOWLEDGMENTS

This work was partially supported by the US Department of Energy, Office of Science, Office of Basic Energy Sciences, the Chemical Sciences, Geosciences, and Biosciences Division under Grant No. DE-FG02-04ER15504. We also acknowledge the partial support of the Ministry of Science and Technology of Taiwan and National Taiwan University (Grants No. 106R104021 and No. 106R8700-2). D.A.T. acknowledges the partial support from the Russian Foundation for Basic Research (Grant No. 16-02-00233).

[1] F. Krausz and M. Ivanov, Rev. Mod. Phys. **81**, 163 (2009).
[2] M. Hentschel, R. Kienberger, C. Spielmann, G. A. Reider, N. Milosevic, T. Brabec, P. Corkum, U. Heinzmann, M. Drescher, and F. Krausz, Nature (London) **414**, 509 (2001).
[3] P. M. Paul, E. S. Toma, P. Breger, G. Mullot, F. Augé, P. Balcou, H. G. Muller, and P. Agostini, Science **292**, 1689 (2001).
[4] Z. Chang, P. B. Corkum, and S. R. Leone, J. Opt. Soc. Am. B **33**, 1081 (2016).
[5] J. Itatani, J. Levesque, D. Zeidler, H. Niikura, H. Pépin, J. C. Kieffer, P. B. Corkum, and D. M. Villeneuve, Nature (London) **432**, 867 (2004).
[6] W. Li, X. Zhou, R. Lock, S. Patchkovskii, A. Stolow, H. C. Kapteyn, and M. M. Murnane, Science **322**, 1207 (2008).
[7] H. Soifer, P. Botheron, D. Shafir, A. Diner, O. Raz, B. D. Bruner, Y. Mairesse, B. Pons, and N. Dudovich, Phys. Rev. Lett. **105**, 143904 (2010).
[8] M. Chini, X. Wang, Y. Cheng, H. Wang, Y. Wu, E. Cunningham, P.-C. Li, J. Heslar, D. A. Telnov, S. I. Chu, and Z. Chang, Nat. Photon. **8**, 437 (2014).
[9] W.-H. Xiong, J.-W. Geng, J.-Y. Tang, L.-Y. Peng, and Q. Gong, Phys. Rev. Lett. **112**, 233001 (2014).
[10] J. Heslar, D. A. Telnov, and S. I. Chu, Phys. Rev. A **93**, 063401 (2016).
[11] W.-H. Xiong, L.-Y. Peng, and Q. Gong, J. Phys. B **50**, 032001 (2017).
[12] P. B. Corkum, Phys. Rev. Lett. **71**, 1994 (1993).
[13] M. Lewenstein, P. Balcou, M. Y. Ivanov, A. L'Huillier, and P. B. Corkum, Phys. Rev. A **49**, 2117 (1994).
[14] X. Chu and S. I. Chu, Phys. Rev. A **63**, 023411 (2001).
[15] G. L. Kamta and A. D. Bandrauk, Phys. Rev. A **71**, 053407 (2005).
[16] D. A. Telnov and S.-I. Chu, Phys. Rev. A **71**, 013408 (2005).
[17] M. Lein, J. Phys. B **40**, R135 (2007).
[18] M. Lein, N. Hay, R. Velotta, J. P. Marangos, and P. L. Knight, Phys. Rev. A **66**, 023805 (2002).
[19] D. A. Telnov and S.-I. Chu, Phys. Rev. A **76**, 043412 (2007).
[20] H. Niikura, F. Légaré, R. Hasbani, A. D. Bandrauk, M. Y. Ivanov, D. M. Villeneuve, and P. B. Corkum, Nature (London) **417**, 917 (2002).
[21] H. Niikura, F. Légaré, R. Hasbani, M. Y. Ivanov, D. M. Villeneuve, and P. B. Corkum, Nature (London) **421**, 826 (2003).
[22] S. Baker, J. S. Robinson, C. A. Haworth, H. Teng, R. A. Smith, C. C. Chirilă, M. Lein, J. W. G. Tisch, and J. P. Marangos, Science **312**, 424 (2006).
[23] S. Baker, J. S. Robinson, M. Lein, C. C. Chirilă, R. Torres, H. C. Bandulet, D. Comtois, J. C. Kieffer, D. M. Villeneuve, J. W. G. Tisch, and J. P. Marangos, Phys. Rev. Lett. **101**, 053901 (2008).

[24] T. Kanai, E. J. Takahashi, Y. Nabekawa, and K. Midorikawa, New J. Phys. **10**, 025036 (2008).
[25] S. Haessler, W. Boutu, M. Stankiewicz, L. J. Frasinsk, S. Weber, J. Caillat, R. Taïeb, A. Maquet, P. Breger, P. Monchicourt, B. Carré, and P. Saliéres, J. Phys. B **42**, 134002 (2009).
[26] A. Zaïr, T. Siegel, S. Sukiasyan, F. Risoud, L. Brugnera, C. Hutchison, Z. Diveki, T. Auguste, J. W. G. Tisch, P. Saliéres, M. Y. Ivanov, and J. P. Marangos, Chem. Phys. **414**, 184 (2013).
[27] C. B. Madsen and L. B. Madsen, Phys. Rev. A **74**, 023403 (2006).
[28] C. C. Chirilă and M. Lein, Phys. Rev. A **77**, 043403 (2008).
[29] M. Y. Emelin, M. Y. Ryabikin, and A. M. Sergeev, New J. Phys. **10**, 025026 (2008).
[30] A. T. Le, T. Morishita, R. R. Lucchese, and C. D. Lin, Phys. Rev. Lett. **109**, 203004 (2012).
[31] L. S. Cederbaum, J. Chem. Phys. **128**, 124101 (2008).
[32] A. Abedi, N. T. Maitra, and E. K. U. Gross, Phys. Rev. Lett. **105**, 123002 (2010).
[33] M. Lein, Phys. Rev. Lett. **94**, 053004 (2005).
[34] A. D. Bandrauk, S. Chelkowski, S. Kawai, and H. Lu, Phys. Rev. Lett. **101**, 153901 (2008).
[35] P. P. Corso, E. Fiordilino, and F. Persico, J. Phys. B **40**, 1383 (2007).
[36] S. Chelkowski, A. Conjusteau, T. Zuo, and A. D. Bandrauk, Phys. Rev. A **54**, 3235 (1996).
[37] Z. B. Walters, S. Tonzani, and C. H. Greene, J. Phys. B **40**, F277 (2007).
[38] Z. B. Walters, S. Tonzani, and C. H. Greene, Chem. Phys. **366**, 103 (2009).
[39] S. Patchkovskii, Phys. Rev. Lett. **102**, 253602 (2009).
[40] S. Patchkovskii and M. S. Schuurman, J. Phys. Chem. A **118**, 12069 (2014).
[41] P. G. Lisinetskaya and R. Mitrić, Phys. Rev. A **83**, 033408 (2011).
[42] M. Falge, V. Engel, and M. Lein, Phys. Rev. A **81**, 023412 (2010).
[43] J. Förster and A. Saenz, Chem. Phys. Chem. **14**, 1438 (2013).
[44] T. Bredtmann, S. Chelkowski, and A. D. Bandrauk, J. Phys. Chem. A **116**, 11398 (2012).
[45] S. Chelkowski, T. Bredtmann, and A. D. Bandrauk, Phys. Rev. A **85**, 033404 (2012).
[46] X. B. Bian and A. D. Bandrauk, Phys. Rev. Lett. **113**, 193901 (2014).
[47] D. A. Telnov, J. Heslar, and S.-I. Chu, Phys. Rev. A **90**, 063412 (2014).
[48] F. Morales, P. Rivière, M. Richter, A. Gubaydullin, M. Ivanov, O. Smirnova, and F. Martín, J. Phys. B **47**, 204015 (2014).
[49] R. E. F. Silva, P. Rivière, F. Morales, O. Smirnova, M. Ivanov, and F. Martín, Sci. Rep. **6**, 32653 (2016).
[50] H. Ahmadi, M. Vafaee, and A. Maghari, J. Phys. B **49**, 035602 (2016).
[51] H. Ahmadi, M. Vafaee, and A. Maghari, Phys. Rev. A **94**, 033415 (2016).
[52] X. M. Tong and S. I. Chu, Chem. Phys. **217**, 119 (1997).
[53] D. A. Telnov and S.-I. Chu, Phys. Rev. A **80**, 043412 (2009).
[54] C. C. Marston and G. G. Balint-Kurti, J. Chem. Phys. **91**, 3571 (1989).
[55] L. Hilico, N. Billy, B. Grémaud, and D. Delande, Eur. Phys. J. D **12**, 449 (2000).
[56] L. D. Landau and E. M. Lifshitz, *The Classical Theory of Fields* (Pergamon Press, Oxford, 1975).
[57] Y. L. Sheu, L. Y. Hsu, H. T. Wu, P.-C. Li, and S.-I. Chu, AIP Adv. **4**, 117138 (2014).
[58] P.-C. Li, Y. L. Sheu, C. Laughlin, and S.-I. Chu, Nat. Commun. **6**, 7178 (2015).
[59] J. Heslar and S.-I. Chu, Sci. Rep. **6**, 37774 (2016).
[60] K. N. Avanaki, D. A. Telnov, and S.-I. Chu, Phys. Rev. A **90**, 033425 (2014).
[61] K. N. Avanaki, D. A. Telnov, H. Z. Jooya, and S.-I. Chu, Phys. Rev. A **92**, 063811 (2015).
[62] R. S. Mulliken, J. Chem. Phys. **7**, 20 (1939).